Circular surface loading on a layered multiferroic half space

2011 Smart Mater. Struct. 20 035020

(http://iopscience.iop.org/0964-1726/20/3/035020)

Smart Mater. Struct. **20** (2011) 035020 (11pp) doi:10.1088/0964-1726/20/3/035020

Circular surface loading on a layered multiferroic half space

H J Chu[1,2], Y Zhang[2], E Pan[2,4] and Q K Han[2,3]

[1] Mechanic Research Group, Yangzhou University, People's Republic of China
[2] Department of Civil Engineering, University of Akron, USA
[3] School of Mechanical Engineering and Automation, Northeastern University, People's Republic of China

E-mail: pan2@ukron.edu

Received 23 June 2010, in final form 11 January 2011
Published 22 February 2011
Online at stacks.iop.org/SMS/20/035020

Abstract
By introducing the cylindrical system of vector functions and the corresponding propagating matrix, we present a semi-analytical solution for a layered multiferroic half space under a uniform vertical circular load on its surface. A two-layered system made of $BaTiO_3$ and $CoFe_2O_4$ is analyzed by the proposed method. The coupling feature among the elastic, electric, and magnetic fields and the interplay between the adjacent layers are investigated. In particular, we find that the interfacial elastic, electric, and magnetic fields are very sensitive to the thickness of the surface layer. Consequently, a critical thickness is found for each field quantity when it reaches its extreme value for varying thickness of the surface layer. This striking feature could be very useful as a theoretical reference for the optimal design of surface coatings.

(Some figures in this article are in colour only in the electronic version)

1. Introduction

Considerable efforts have been devoted to multiferroic composites made of piezoelectric and piezomagnetic materials due to their broad applications related to smart systems such as intelligent sensors, damage detectors, etc (Spaldin and Fiebig 2005, Fiebig 2005, Kohlstedt *et al* 2005, Ramesh and Spaldin 2007, Rogez *et al* 2010). Since multiferroic materials/composites possess at least two coexisting orders among the magnetic, electric, and elastic fields, they may also play an important role in future magnetic applications (Kimura *et al* 2003, Zhuravlev *et al* 2005). It is possible to fabricate multiferroic composites by artificially making ferroelectric and ferromagnetic heterostructures in the nanoscale (Zhong *et al* 2008). The interplay among elastic, electric, and magnetic fields also provides excellent alternative avenues for controlling material growth or optimizing material properties (Kimura *et al* 2003, Lottermoser *et al* 2004, Duan *et al* 2006, Pang *et al* 2010, Sun and Kim 2010).

The complex coupling effect in multiferroic materials/composites was investigated before. These include the studies on the peculiar magneto-electric effect (Nan 1994, Benveniste 1995, Wu and Huang 2000, Liu *et al* 2004) as well as the general effective properties of composites (Li and Dunn 1998), static and dynamic structural behavior (Pan 2001, Chen *et al* 2004, Ramirez 2006, Ke *et al* 2008, Wang *et al* 2010), fracture-mechanics-related problems (Liu *et al* 2001, Sih and Chen 2003, Feng *et al* 2007, Zhong 2009, Zhong *et al* 2009, Rungamornrat and Senjuntichai 2009), and on the general coupling theory based on Green's function and other mathematical approaches (Pan 2002, Wang and Shen 2002, Li 2003, Hou *et al* 2005, Wang *et al* 2008, Feng *et al* 2009).

Circular surface loading on multilayered half spaces is a very interesting boundary value problem. It has important practical applications in various engineering areas, such as cell biology (Balaban *et al* 2001, Schwarz *et al* 2002), smart piezoelectric composites (Pan and Han 2005, Han *et al* 2006), foundation engineering (Graig 1997), and earth science (Becker and Bevis 2004, Pan *et al* 2007). Combined with the Hertzian contact theory, the surface loading solution can be utilized in indentation tests for material characterization (Xu *et al* 1999, Yu 2001, Giannakopoulos and Suresh 1999, Chen *et al* 2010). Numerous analytical and/or numerical methods were proposed in the past for solving the circular loading problem in inhomogeneous elastic isotropic (Oner 1990, Yue *et al* 1999) and elastic non-isotropic (Hooper 1975, Rowe and Booker 1981, Kumar 1988, Doherty and Deeks 2003,

[4] Author to whom any correspondence should be addressed.

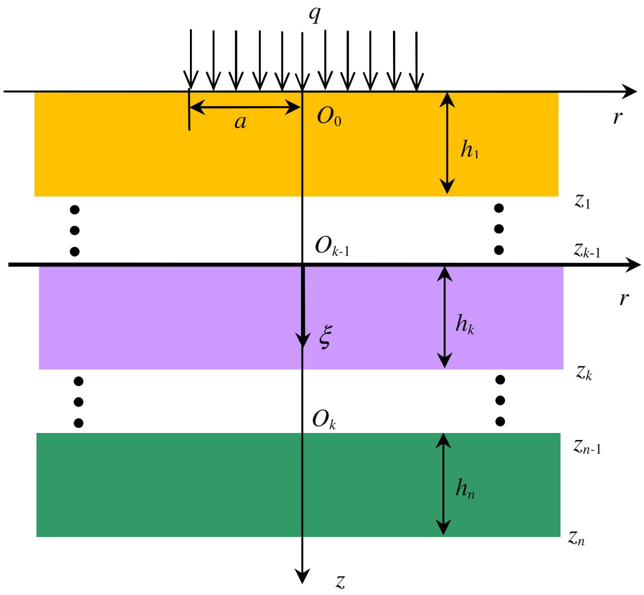

Figure 1. Schematic of a layered magneto-electro-elastic half space under a uniform surface loading over a circular area. The global coordinate system is (r, θ, z) with the origin O_0, and the local coordinate system in the kth layer is (r, θ, ξ) with the origin O_{k-1}.

Wang *et al* 2005) structures. To the best knowledge of the authors, however, the surface loading problem corresponding to a layered multiferroic half space has not been reported in the literature.

Thus, in this paper, we focus on the response of a transversely isotropic and layered multiferroic half space under a uniform vertical load within a circle on its surface. The solution is derived by virtue of the cylindrical system of vector functions and the propagator matrix method (Gilbert and Backus 1966, Ulitko 1979, Pan 1989). First, we transform the basic equations in the physical domain to the transformed domain in terms of the cylindrical system of vector functions. Secondly, making use of the boundary conditions, we obtain the exact solutions of this problem in the transformed domain. Thirdly, the solutions in the transformed domain are inverted back to the physical domain, and the semi-analytical solutions including one-dimensional integration are obtained. Finally, the proposed method is applied to a two-layered half space made of piezoelectric $BaTiO_3$ and magnetic $CoFe_2O_4$. Besides some interesting coupling features among the elastic, electric, and magnetic fields, our numerical results show further some peculiar interplay behavior between the adjacent layers and the influence of the thickness of the surface layer on the field quantities. In particular, the critical thickness of the surface layer is introduced to analyze the field variation feature, which could provide an important theoretical guidance to future practical design of layered structures made of the novel multiferroic materials/composites.

2. Basic equations and cylindrical system of vector functions

Consider a magneto-electro-elastic layered half space under a uniform vertical load q over a circle of radius a, as shown in figure 1. Two cylindrical coordinates, i.e. global coordinates (r, θ, z) and local coordinates (r, θ, ξ), are attached to the layered half space. Due to the translation relationship between the global and local coordinates, we have $\partial()/\partial z = \partial()/\partial \xi$ which implies that the basic equations (e.g. the constitutive relations, equilibrium equations, etc) under global and local coordinates have the same form.

Under the global coordinates, the constitutive relations of the magneto-electro-elastic material are (in terms of the material coefficients)

$$\begin{aligned}
\sigma_{rr} &= c_{11}\gamma_{rr} + c_{12}\gamma_{\theta\theta} + c_{13}\gamma_{zz} - e_{31}E_z - q_{31}H_z \\
\sigma_{\theta\theta} &= c_{12}\gamma_{rr} + c_{11}\gamma_{\theta\theta} + c_{13}\gamma_{zz} - e_{31}E_z - q_{31}H_z \\
\sigma_{zz} &= c_{13}\gamma_{rr} + c_{13}\gamma_{\theta\theta} + c_{33}\gamma_{zz} - e_{33}E_z - q_{33}H_z \\
\sigma_{\theta z} &= 2c_{44}s_{\theta z} - e_{15}E_\theta - q_{15}H_\theta \\
\sigma_{rz} &= 2c_{44}\gamma_{rz} - e_{15}E_r - q_{15}H_r \\
\sigma_{r\theta} &= 2c_{66}\gamma_{r\theta}
\end{aligned} \tag{1a}$$

$$\begin{aligned}
D_r &= 2e_{15}\gamma_{rz} + \varepsilon_{11}E_r + d_{11}H_r \\
D_\theta &= 2e_{15}\gamma_{\theta z} + \varepsilon_{11}E_\theta + d_{11}H_\theta \\
D_z &= e_{31}(\gamma_{rr} + \gamma_{\theta\theta}) + e_{33}\gamma_{zz} + \varepsilon_{33}E_z + d_{33}H_z
\end{aligned} \tag{1b}$$

$$\begin{aligned}
B_r &= 2q_{15}\gamma_{rz} + d_{11}E_r + \mu_{11}H_r \\
B_\theta &= 2q_{15}\gamma_{\theta z} + d_{11}E_\theta + \mu_{11}H_\theta \\
B_z &= q_{31}(\gamma_{rr} + \gamma_{\theta\theta}) + q_{33}\gamma_{zz} + d_{33}E_z + \mu_{33}H_z
\end{aligned} \tag{1c}$$

where σ_{ij}, D_i, and B_i $(i, j = r, \theta, \xi)$ are the elastic stresses, electrical displacements, and magnetic fields, respectively; γ_{ij}, E_i, and H_i denote the elastic strains, electric fields, and magnetizing fields, respectively.

The generalized equilibrium equations of the magneto-electro-elastic material without 'body forces' are

$$\begin{aligned}
&\frac{\partial\sigma_{rr}}{\partial r} + \frac{1}{r}\frac{\partial\sigma_{r\theta}}{\partial\theta} + \frac{\partial\sigma_{rz}}{\partial z} + \frac{\sigma_{rr} - \sigma_{\theta\theta}}{r} = 0, \\
&\frac{\partial\sigma_{r\theta}}{\partial r} + \frac{1}{r}\frac{\partial\sigma_{\theta\theta}}{\partial\theta} + \frac{\partial\sigma_{\theta z}}{\partial z} + \frac{2\sigma_{r\theta}}{r} = 0, \\
&\frac{\partial\sigma_{rz}}{\partial r} + \frac{1}{r}\frac{\partial\sigma_{\theta z}}{\partial\theta} + \frac{\partial\sigma_{zz}}{\partial z} + \frac{\sigma_{rz}}{r} = 0, \\
&\frac{\partial D_r}{\partial r} + \frac{1}{r}\frac{\partial D_\theta}{\partial\theta} + \frac{\partial D_z}{\partial z} + \frac{D_r}{r} = 0, \\
&\frac{\partial B_r}{\partial r} + \frac{1}{r}\frac{\partial B_\theta}{\partial\theta} + \frac{\partial B_z}{\partial z} + \frac{B_r}{r} = 0.
\end{aligned} \tag{2}$$

In order to solve the problem, the cylindrical system of vector functions is introduced (Ulitko 1979, Pan 1989)

$$\begin{aligned}
\mathbf{L}(r, \theta; \lambda, m) &= \mathbf{i}_z S(r, \theta; \lambda, m) \\
\mathbf{M}(r, \theta; \lambda, m) &= \nabla S = \mathbf{i}_r \frac{\partial S}{\partial r} + \mathbf{i}_\theta \frac{\partial S}{r\partial\theta} \\
\mathbf{N}(r, \theta; \lambda, m) &= \nabla \times (\mathbf{i}_z S) = \mathbf{i}_r \frac{\partial S}{r\partial\theta} - \mathbf{i}_\theta \frac{\partial S}{\partial r}
\end{aligned} \tag{3}$$

with

$$S(r, \theta; \lambda, m) = \frac{1}{\sqrt{2\pi}} J_m(\lambda r)\exp(im\theta) \tag{4}$$

where $\mathbf{i}_r$, $\mathbf{i}_\theta$, and $\mathbf{i}_z$ are the unit vectors in cylindrical coordinates and $J_m(\lambda r)$ denotes the Bessel function of order m. The function S satisfies

$$\frac{\partial^2 S}{\partial r^2}+\frac{1}{r^2}\frac{\partial^2 S}{\partial\theta^2}+\frac{1}{r}\frac{\partial S}{\partial r}+\lambda^2 S=0. \tag{5}$$

Due to the orthogonal properties of $\mathbf{L}$, $\mathbf{M}$, and $\mathbf{N}$ defined in equations (3), the elastic displacements, electric and magnetic potentials can be expressed in terms of these vector functions as

$$\begin{aligned}\mathbf{u}(r,\theta,z)&=\sum_m\int_0^{+\infty}(U_L\mathbf{L}+U_M\mathbf{M}+U_N\mathbf{N})\,\lambda\,\mathrm{d}\lambda\\ \phi(r,\theta,z)&=\sum_m\int_0^{+\infty}\Phi S\lambda\,\mathrm{d}\lambda\\ \psi(r,\theta,z)&=\sum_m\int_0^{+\infty}\Psi S\lambda\,\mathrm{d}\lambda\end{aligned}\tag{6}$$

where the expansion coefficients U_L, U_M, U_N, Φ, and Ψ are functions of (z,λ,m). Similarly, we can find the following expansions

$$\begin{aligned}\mathbf{T}(r,\theta,z)&\equiv\sigma_{rz}\mathbf{i}_r+\sigma_{\theta z}\mathbf{i}_\theta+\sigma_{zz}\mathbf{i}_z\\ &=\sum_m\int_0^{+\infty}(T_L\mathbf{L}+T_M\mathbf{M}+T_N\mathbf{N})\,\lambda\,\mathrm{d}\lambda\\ \mathbf{D}(r,\theta,z)&=\sum_m\int_0^{+\infty}(D_L\mathbf{L}+D_M\mathbf{M}+D_N\mathbf{N})\,\lambda\,\mathrm{d}\lambda\\ \mathbf{B}(r,\theta,z)&=\sum_m\int_0^{+\infty}(B_L\mathbf{L}+B_M\mathbf{M}+B_N\mathbf{N})\,\lambda\,\mathrm{d}\lambda.\end{aligned}\tag{7}$$

Unless otherwise indicated, the summation of m and integration of $\int_0^\infty[\ ]\lambda\,\mathrm{d}\lambda$ will be omitted in the following derivation. Based on equation (6) and making use of equations (5) and (1) we obtain

$$\begin{aligned}\sigma_{rr}&=c_{11}\left(U_M\frac{\partial^2 S}{\partial r^2}-\frac{U_N}{r^2}\frac{\partial S}{\partial\theta}+\frac{U_N}{r}\frac{\partial^2 S}{\partial r\partial\theta}\right)\\ &\quad+c_{12}\left(\frac{U_M}{r^2}\frac{\partial^2 S}{\partial\theta^2}-\frac{U_N}{r}\frac{\partial^2 S}{\partial r\partial\theta}+\frac{U_M}{r}\frac{\partial S}{\partial r}+\frac{U_N}{r^2}\frac{\partial S}{\partial\theta}\right)\\ &\quad+c_{13}\left(\frac{\partial U_L}{\partial z}S\right)+e_{31}\frac{\partial\Phi}{\partial z}S+q_{31}\frac{\partial\Psi}{\partial z}S\end{aligned}\tag{8a}$$

$$\begin{aligned}\sigma_{\theta\theta}&=c_{12}\left(U_M\frac{\partial^2 S}{\partial r^2}-\frac{U_N}{r^2}\frac{\partial S}{\partial\theta}+\frac{U_N}{r}\frac{\partial^2 S}{\partial r\partial\theta}\right)\\ &\quad+c_{11}\left(\frac{U_M}{r^2}\frac{\partial^2 S}{\partial\theta^2}-\frac{U_N}{r}\frac{\partial^2 S}{\partial r\partial\theta}+\frac{U_M}{r}\frac{\partial S}{\partial r}+\frac{U_N}{r^2}\frac{\partial S}{\partial\theta}\right)\\ &\quad+c_{13}\left(\frac{\partial U_L}{\partial z}S\right)+e_{31}\frac{\partial\Phi}{\partial z}S+q_{31}\frac{\partial\Psi}{\partial z}S\end{aligned}\tag{8b}$$

$$\begin{aligned}\sigma_{zz}&=c_{13}\left(U_M\frac{\partial^2 S}{\partial r^2}-\frac{U_N}{r^2}\frac{\partial S}{\partial\theta}+\frac{U_N}{r}\frac{\partial^2 S}{\partial r\partial\theta}\right)\\ &\quad+c_{13}\left(\frac{U_M}{r^2}\frac{\partial^2 S}{\partial\theta^2}-\frac{U_N}{r}\frac{\partial^2 S}{\partial r\partial\theta}+\frac{U_M}{r}\frac{\partial S}{\partial r}+\frac{U_N}{r^2}\frac{\partial S}{\partial\theta}\right)\\ &\quad+c_{33}\left(\frac{\partial U_L}{\partial z}S\right)+e_{33}\frac{\partial\Phi}{\partial z}S+q_{33}\frac{\partial\Psi}{\partial z}S\end{aligned}\tag{8c}$$

$$\begin{aligned}\sigma_{\theta z}&=c_{44}\left(\frac{\partial U_M}{\partial z}\frac{\partial S}{r\partial\theta}-\frac{\partial U_N}{\partial z}\frac{\partial S}{\partial r}+\frac{U_L}{r}\frac{\partial S}{\partial\theta}\right)\\ &\quad+e_{15}\frac{\Phi}{r}\frac{\partial S}{\partial\theta}+q_{15}\frac{\Psi}{r}\frac{\partial S}{\partial\theta}\\ \sigma_{rz}&=c_{44}\left(U_L\frac{\partial S}{\partial r}+\frac{\partial U_M}{\partial z}\frac{\partial S}{\partial r}+\frac{\partial U_N}{\partial z}\frac{\partial S}{r\partial\theta}\right)\\ &\quad+e_{15}\Phi\frac{\partial S}{\partial r}+q_{15}\Psi\frac{\partial S}{\partial r}\\ \sigma_{r\theta}&=c_{66}\left(\frac{2U_M}{r}\frac{\partial^2 S}{\partial r\partial\theta}+\frac{U_N}{r^2}\frac{\partial^2 S}{\partial\theta^2}-\frac{2U_M}{r^2}\frac{\partial S}{\partial\theta}\right.\\ &\quad\left.-U_N\frac{\partial^2 S}{\partial r^2}+\frac{U_N}{r}\frac{\partial S}{\partial r}\right)\end{aligned}\tag{8d}$$

$$\begin{aligned}D_r&=e_{15}\left(U_L\frac{\partial S}{\partial r}+\frac{\partial U_M}{\partial z}\frac{\partial S}{\partial r}+\frac{\partial U_N}{\partial z}\frac{\partial S}{r\partial\theta}\right)\\ &\quad-\varepsilon_{11}\Phi\frac{\partial S}{\partial r}-d_{11}\Psi\frac{\partial S}{\partial r}\\ D_\theta&=e_{15}\left(\frac{U_L}{r}\frac{\partial S}{\partial\theta}+\frac{\partial U_M}{\partial z}\frac{\partial S}{r\partial\theta}-\frac{\partial U_N}{\partial z}\frac{\partial S}{\partial r}\right)\\ &\quad-\varepsilon_{11}\frac{\Phi}{r}\frac{\partial S}{\partial\theta}-d_{11}\frac{\Psi}{r}\frac{\partial S}{\partial\theta}\\ D_z&=-\lambda^2 e_{31}U_M S+e_{33}\frac{\partial U_L}{\partial z}S-\varepsilon_{33}\frac{\partial\Phi}{\partial z}S-d_{33}\frac{\partial\Psi}{\partial z}S\end{aligned}\tag{8e}$$

$$\begin{aligned}B_r&=q_{15}\left(U_L\frac{\partial S}{\partial r}+\frac{\partial U_M}{\partial z}\frac{\partial S}{\partial r}+\frac{\partial U_N}{\partial z}\frac{\partial S}{r\partial\theta}\right)\\ &\quad-d_{11}\Phi\frac{\partial S}{\partial r}-\mu_{11}\Psi\frac{\partial S}{\partial r}\\ B_\theta&=q_{15}\left(\frac{U_L}{r}\frac{\partial S}{\partial\theta}+\frac{\partial U_M}{\partial z}\frac{\partial S}{r\partial\theta}-\frac{\partial U_N}{\partial z}\frac{\partial S}{\partial r}\right)\\ &\quad-d_{11}\frac{\Phi}{r}\frac{\partial S}{\partial\theta}-\mu_{11}\frac{\Psi}{r}\frac{\partial S}{\partial\theta}\\ B_z&=-\lambda^2 q_{31}U_M S+q_{33}\frac{\partial U_L}{\partial z}S-d_{33}\frac{\partial\Phi}{\partial z}S-\mu_{33}\frac{\partial\Psi}{\partial z}S.\end{aligned}\tag{8f}$$

Substituting equation (8) into (2), we obtain five equilibrium equations in terms of the expansion coefficients. Comparing equations (8) and (7) provides another five equations. Therefore, there are in total ten equations, which can be further recast into two independent sets of linear differential equations called Group I and Group II. In Group I, these equations are

$$\begin{aligned}T_L&=-\lambda^2 c_{13}U_M+c_{33}\frac{\partial U_L}{\partial z}+e_{33}\frac{\partial\Phi}{\partial z}+q_{33}\frac{\partial\Psi}{\partial z}\\ T_M&=c_{44}\left(U_L+\frac{\partial U_M}{\partial z}\right)+e_{15}\Phi+q_{15}\Psi\\ D_L&=-e_{31}\lambda^2 U_M+e_{33}\frac{\partial U_L}{\partial z}-\varepsilon_{33}\frac{\partial\Phi}{\partial z}-d_{33}\frac{\partial\Psi}{\partial z}\\ B_L&=-q_{31}\lambda^2 U_M+q_{33}\frac{\partial U_L}{\partial z}-d_{33}\frac{\partial\Phi}{\partial z}-\mu_{33}\frac{\partial\Psi}{\partial z}\end{aligned}\tag{9a}$$

$$\frac{\partial T_L}{\partial z} - \lambda^2 T_M = 0$$

$$\frac{\partial T_M}{\partial z} - \lambda^2 c_{11} U_M + c_{13}\frac{\partial U_L}{\partial z} + e_{31}\frac{\partial \Phi}{\partial z} + q_{31}\frac{\partial \Psi}{\partial z} = 0$$

$$\frac{\partial D_L}{\partial z} - \lambda^2 e_{15}\left(\frac{\partial U_M}{\partial z} + U_L\right) + \lambda^2 \varepsilon_{11}\Phi + \lambda^2 d_{11}\Psi = 0$$

$$\frac{\partial B_L}{\partial z} - \lambda^2 q_{15}\left(\frac{\partial U_M}{\partial z} + U_L\right) + \lambda^2 d_{11}\Phi + \lambda^2 \mu_{11}\Psi = 0 \qquad (9b)$$

and in Group II they are

$$\frac{\partial T_N}{\partial z} - \lambda^2 c_{66} U_N = 0 \qquad T_N = c_{44}\frac{\partial U_N}{\partial z}. \qquad (10)$$

3. Propagating matrix in each layer

The local coordinates will be used in this section. As mentioned before, due to the translation relationship between the global and local coordinates, equations (1)–(10) hold if the partial derivative $\partial/\partial z$ is replaced by $\partial/\partial \xi$.

It is easy to find the general solution of equation (10) in any layer (i.e. the kth layer) using the local coordinates. The solution of Group II is

$$\left[\mathbf{P}_k^{\mathrm{II}}(\xi)\right] = \left[\mathbf{B}_k^{\mathrm{II}}\right] \mathrm{diag}\left[\mathrm{e}^{\lambda s_k \xi}, \mathrm{e}^{-\lambda s_k \xi}\right]\left[\mathbf{K}_k^{\mathrm{II}}\right] \qquad (11)$$

where

$$\left[\mathbf{P}_k^{\mathrm{II}}(\xi)\right] \equiv \left[U_N^k(\xi), \quad T_N^k(\xi)/\lambda\right]^{\mathrm{T}} \qquad (12)$$

$$\left[\mathbf{B}_k^{\mathrm{II}}\right] = \begin{bmatrix} 1 & 1 \\ \bar{s}_k & -\bar{s}_k \end{bmatrix}, \qquad s_k = \sqrt{c_{66}^k / c_{44}^k}, \qquad \bar{s}_k = \sqrt{c_{44}^k c_{66}^k}, \qquad (13)$$

and the subscript and superscript 'k' denotes the corresponding variables or coefficients in the kth layer (e.g. c_{44}^k and c_{66}^k are the elastic constants of the kth layer). Also in equation (11), $[\mathbf{K}_k^{\mathrm{II}}]$ is a 2×1 column matrix with the unknown coefficients being determined by the boundary/interface conditions. Actually, equation (11) can be equivalently expressed as

$$[\mathbf{P}_k^{\mathrm{II}}(\xi)] = [\mathbf{B}_k^{\mathrm{II}}]\mathrm{diag}[\mathrm{e}^{\lambda s_k(\xi - h_k)}, \mathrm{e}^{-\lambda s_k(\xi - h_k)}] \times [\mathbf{B}_k^{\mathrm{II}}]^{-1}[\mathbf{P}_k^{\mathrm{II}}(h_k)]. \qquad (14)$$

Assuming that the continuity conditions hold at the interface ($z = z_{k-1}$) between the adjacent layers, we then have

$$\left[\mathbf{P}_k^{\mathrm{II}}(0)\right] = \left[\mathbf{P}_{k-1}^{\mathrm{II}}(h_{k-1})\right]. \qquad (15)$$

Hence, the propagating relation between two adjacent layers is

$$\left[\mathbf{P}_{k-1}^{\mathrm{II}}(h_{k-1})\right] = \left[\mathbf{a}_k^{\mathrm{II}}\right]\left[\mathbf{P}_k^{\mathrm{II}}(h_k)\right] \qquad (16)$$

with

$$\left[\mathbf{a}_k^{\mathrm{II}}\right] = \begin{bmatrix} \cosh(\lambda s_k h_k) & -\sinh(\lambda s_k h_k)/\bar{s}_k \\ -\bar{s}_k \sinh(\lambda s_k h_k) & \cosh(\lambda s_k h_k) \end{bmatrix}$$

being the propagator, or propagating matrix, which relates the components U_N and T_N at the two interfaces $z = z_{k-1}$ and z_k.

Similar to equation (12), we define, for Group II,

$$\left[\mathbf{P}_k^{\mathrm{I}}\right] \equiv [U_L^k, \lambda U_M^k, T_L^k/\lambda, T_M^k, \Phi^k, \Psi^k, D_L^k/\lambda, B_L^k/\lambda]^{\mathrm{T}}. \qquad (17)$$

Then equations (9) can be expressed as

$$\left[\mathbf{P}_k^{\mathrm{I}}(\xi)\right]_{,z} = \lambda[\mathbf{W}_k]\left[\mathbf{P}_k^{\mathrm{I}}(\xi)\right] \qquad (18)$$

where $[\mathbf{W}_k]$ is an 8×8 matrix and its nonzero elements are listed in the appendix. It should be noted that the matrix $[\mathbf{W}_k]$ depends only on the material constants of the kth layer; in other words, it is independent of the vertical coordinate z or ξ and the transformation variables m and λ. Hence, the general solution of equation (18) can be assumed as

$$\left[\mathbf{P}_k^{\mathrm{I}}(\xi)\right] = [\mathbf{b}^k]\exp\left(\lambda \nu^k \xi\right). \qquad (19)$$

Substituting equation (19) into (18), we have

$$\left\{[\mathbf{W}_k] - \nu^k[\mathbf{I}]\right\}[\mathbf{b}^k] = 0 \qquad (20)$$

where $[\mathbf{I}]$ is an 8×8 identity matrix. Obviously, the eigenvalues ν_i^k ($i = 1, 2, \ldots, 8$) and corresponding eigenvectors $\mathbf{b}_i^k$ ($i = 1, 2, \ldots, 8$) of equation (20) depend on the property of the matrix $[\mathbf{W}_k]$. Assuming that the eigenvalues are distinct, the general solution of equation (19) can be expressed as

$$\left[\mathbf{P}_k^{\mathrm{I}}(\xi)\right] = [\mathbf{B}_k^{\mathrm{I}}]\langle \mathrm{e}^{\lambda \nu_*^k \xi}\rangle\left[\mathbf{K}_k^{\mathrm{I}}\right] \qquad (21)$$

with

$$[\mathbf{B}_k^{\mathrm{I}}] = [\mathbf{b}_1^k, \mathbf{b}_2^k, \mathbf{b}_3^k, \mathbf{b}_4^k, \mathbf{b}_5^k, \mathbf{b}_6^k, \mathbf{b}_7^k, \mathbf{b}_8^k]$$

$$\langle \mathrm{e}^{\lambda \nu_*^k \xi}\rangle = \mathrm{diag}\left[\mathrm{e}^{\lambda \nu_1^k \xi}, \mathrm{e}^{\lambda \nu_2^k \xi}, \mathrm{e}^{\lambda \nu_3^k \xi}, \mathrm{e}^{\lambda \nu_4^k \xi}, \mathrm{e}^{\lambda \nu_5^k \xi}, \mathrm{e}^{\lambda \nu_6^k \xi}, \mathrm{e}^{\lambda \nu_7^k \xi}, \mathrm{e}^{\lambda \nu_8^k \xi}\right] \qquad (22)$$

where $[\mathbf{K}_k^{\mathrm{I}}]$ is an 8×1 coefficient matrix to be determined by the interface and/or boundary conditions.

Similar to Group I, we can derive

$$\left[\mathbf{P}_{k-1}^{\mathrm{I}}(h_{k-1})\right] = [\mathbf{a}_k^{\mathrm{I}}]\left[\mathbf{P}_k^{\mathrm{I}}(h_k)\right] \qquad (23)$$

with

$$[\mathbf{a}_k^{\mathrm{I}}] = [\mathbf{B}_k^{\mathrm{I}}]\langle \mathrm{e}^{-\lambda \nu_*^k h_k}\rangle[\mathbf{B}_k^{\mathrm{I}}]^{-1} \qquad (24)$$

being the propagator or propagating matrix which connects the values $[\mathbf{P}_k^{\mathrm{I}}]$ at the two interfaces $z = z_{k-1}$ and z_k.

We can now propagate the propagating relations (16) and (23) from the bottom layer to the top. By further making use of equations (11) and (21) for the homogeneous half space (i.e. the last layer), we obtain the following important relations in the transformed domain

$$\begin{aligned} [\mathbf{P}_0^{\mathrm{I}}(0)] &= [\mathbf{a}_1^{\mathrm{I}}][\mathbf{a}_2^{\mathrm{I}}]\cdots[\mathbf{a}_{n-1}^{\mathrm{I}}][\mathbf{B}_n^{\mathrm{I}}][\mathbf{K}_n^{\mathrm{I}}] \equiv [\Pi^{\mathrm{I}}][\mathbf{K}_n^{\mathrm{I}}] \\ [\mathbf{P}_0^{\mathrm{II}}(0)] &= [\mathbf{a}_1^{\mathrm{II}}][\mathbf{a}_2^{\mathrm{II}}]\cdots[\mathbf{a}_{n-1}^{\mathrm{II}}][\mathbf{B}_n^{\mathrm{II}}][\mathbf{K}_n^{\mathrm{II}}] \equiv [\Pi^{\mathrm{II}}][\mathbf{K}_n^{\mathrm{II}}] \end{aligned} \qquad (25)$$

where n denotes the last layer and 0 the surface layer. Equation (25) may be recast into

$$\begin{bmatrix} \mathbf{P}^{\mathrm{I}}(0) \\ \mathbf{P}^{\mathrm{II}}(0) \end{bmatrix} = \begin{bmatrix} \Pi^{\mathrm{I}} & \mathbf{0} \\ \mathbf{0} & \Pi^{\mathrm{II}} \end{bmatrix}\begin{bmatrix} \mathbf{K}_n^{\mathrm{I}} \\ \mathbf{K}_n^{\mathrm{II}} \end{bmatrix} \qquad (26)$$

with the unknown coefficients $[\mathbf{K}_k^{\mathrm{I}}]$ and $[\mathbf{K}_n^{\mathrm{II}}]$ being determined by the boundary conditions at the surface and the requirement that the solution is finite in the homogeneous half space, as discussed below.

4. Solutions in transformed and physical domains

Applying equations (11) and (21) to the last layer, i.e. the nth layer made of the homogeneous half space, and considering the requirement that the solution should vanish as z or ξ approaches $+\infty$, we find that the undetermined coefficient matrices should have the following structure

$$\begin{aligned}[\mathbf{K}_k^{\mathrm{I}}] &= [0, 0, 0, 0, p_1, p_2, p_3, p_4]^{\mathrm{T}} \\ [\mathbf{K}_k^{\mathrm{II}}] &= [\,0, \quad p_5\,]^{\mathrm{T}}\end{aligned} \tag{27}$$

where p_i ($i = 1$–5) are the unknown coefficients to be determined. These five unknown coefficients can be determined by using the surface boundary conditions at $z = 0$.

Under a uniform vertical load within a circle of radius a as in figure 1, the mechanical boundary conditions on the surface are

$$\begin{aligned}\sigma_{zz}(r, \theta, 0) &= q, & r &\in [0, a] \\ \sigma_{zz}(r, \theta, 0) &= 0, & r &\in (a, \infty) \\ \sigma_{rz}(r, \theta, 0) &= 0, & r &\in [0, \infty) \\ \sigma_{\theta z}(r, \theta, 0) &= 0, & r &\in [0, \infty).\end{aligned} \tag{28}$$

The electric and magnetic boundary conditions are

$$\begin{aligned}D_z(r, \theta, 0) &= 0, & r &\in [0, \ \infty) \\ B_z(r, \theta, 0) &= 0, & r &\in [0, \ \infty).\end{aligned} \tag{29}$$

Based on the inverse transform of equation (7), equations (28) and (29) can be transformed into

$$\begin{aligned}T_L(0) &= \frac{\sqrt{2\pi}a}{\lambda} J_1(a\lambda) \\ T_M(0) &= T_N(0) = D_L(0) = B_L(0) = 0.\end{aligned} \tag{30}$$

Substituting equation (30) into (26), we arrive at five equations with the five unknown coefficients in equation (27) being included, i.e.

$$\begin{bmatrix} \Pi^{\mathrm{II}}(3,5) & \Pi^{\mathrm{II}}(3,6) & \Pi^{\mathrm{II}}(3,7) & \Pi^{\mathrm{II}}(3,8) & 0 \\ \Pi^{\mathrm{II}}(4,5) & \Pi^{\mathrm{II}}(4,6) & \Pi^{\mathrm{II}}(4,7) & \Pi^{\mathrm{II}}(3,8) & 0 \\ \Pi^{\mathrm{II}}(7,5) & \Pi^{\mathrm{II}}(7,6) & \Pi^{\mathrm{II}}(7,7) & \Pi^{\mathrm{II}}(7,8) & 0 \\ \Pi^{\mathrm{II}}(8,5) & \Pi^{\mathrm{II}}(8,6) & \Pi^{\mathrm{II}}(8,7) & \Pi^{\mathrm{II}}(8,8) & 0 \\ 0 & 0 & 0 & 0 & \Pi^{\mathrm{I}}(2,2) \end{bmatrix} \times \begin{bmatrix} p_1 \\ p_2 \\ p_3 \\ p_4 \\ p_5 \end{bmatrix} = \sqrt{2\pi} \begin{bmatrix} \frac{a}{\lambda^2} J_1(a\lambda) \\ 0 \\ 0 \\ 0 \\ 0 \end{bmatrix}. \tag{31}$$

Therefore, from equation (31), one can easily solve the coefficients p_i ($i = 1$–5). With these coefficients, solutions at any z-level or any interface ($z = z_k$) can be solved. For instance, the solution at any interface ($z = z_k$) in the transformed domain can be expressed exactly as

$$\begin{aligned}[\mathbf{P}_k^{\mathrm{I}}(z_k)] &= [\mathbf{a}_{k+1}^{\mathrm{I}}][\mathbf{a}_{k+2}^{\mathrm{I}}]\cdots[\mathbf{a}_{n-1}^{\mathrm{I}}][\mathbf{B}_n^{\mathrm{I}}][\mathbf{K}_n^{\mathrm{I}}] \\ [\mathbf{P}_k^{\mathrm{II}}(z_k)] &= [\mathbf{a}_{k+1}^{\mathrm{II}}][\mathbf{a}_{k+2}^{\mathrm{II}}]\cdots[\mathbf{a}_{n-1}^{\mathrm{II}}][\mathbf{B}_n^{\mathrm{II}}][\mathbf{K}_n^{\mathrm{II}}]\end{aligned} \tag{32}$$

Table 1. Nonzero material coefficients of the piezoelectric $BaTiO_3$ (c_{ij} in 10^9 N m^{-2}, e_{ij} in C m^{-2}, ε_{ij} in 10^{-9} C^2 N^{-1} m^{-2}, μ_{ij} in 10^{-6} N s^2 C^{-2}).

c_{11}	c_{12}	c_{13}	c_{33}	c_{44}	μ_{11}
166	77	78	162	43	5
e_{31}	e_{33}	e_{15}	ε_{11}	ε_{33}	μ_{33}
−4.4	18.6	11.6	11.2	12.6	10

and the solutions at any vertical level within, say the kth layer, are

$$\begin{aligned}[\mathbf{P}_k^{\mathrm{I}}(\xi)] &= [\mathbf{B}_k^{\mathrm{I}}]\langle \mathrm{e}^{\lambda v_*^k(\xi-h_k)}\rangle[\mathbf{B}_k^{\mathrm{I}}]^{-1}[\mathbf{P}_k^{\mathrm{I}}(z_k)] \\ [\mathbf{P}_k^{\mathrm{II}}(\xi)] &= [\mathbf{B}_k^{\mathrm{II}}]\mathrm{diag}[\mathrm{e}^{\lambda s_k(\xi-h_k)}, \mathrm{e}^{-\lambda s_k(\xi-h_k)}][\mathbf{B}_k^{\mathrm{II}}]^{-1}[\mathbf{P}_k^{\mathrm{II}}(z_k)].\end{aligned} \tag{33}$$

Recalling the definition for $[\mathbf{P}_k^{\mathrm{I}}]$ and $[\mathbf{P}_k^{\mathrm{II}}]$, together with equations (33), we can obtain the elastic displacements and electric and magnetic potentials in the transformed domain. Based on equations (8), the stress field and electric and magnetic fields can also be determined.

The exact solutions obtained above in the transformed domain need to be transformed inversely back to the physical domain. The general transform expression for any given vector function $\boldsymbol{f}$ is

$$\mathbf{f}(r, \theta, z) = \sum_m \int_0^{+\infty} [F_L(z, \lambda, m)\mathbf{L} + F_M(z, \lambda, m)\mathbf{M} + F_N(z, \lambda, m)\mathbf{N}]\lambda\,\mathrm{d}\lambda \tag{34}$$

where $\boldsymbol{f}(r, \theta, z)$ denotes the function in the physical domain, F_L, F_M, and F_N denote the corresponding components in the transformed domain.

Using equation (34), together with equations (33), (6), and (7), the solution in the physical domain can be derived. Generally, due to the complicated properties of the layered structure such as material anisotropy and coupling among elastic, electric, and magnetic fields, numerical integrations are needed in order to obtain the solution in the physical domain. The numerical integral is carried out based on an adaptive numerical quadrature scheme (see, e.g. Pan and Han 2005).

5. Numerical results and analyses

In our numerical studies, the layered magneto-electro-elastic half space is made of two transversely isotropic materials. The first layer is piezoelectric material $BaTiO_3$ and the second layer (i.e. the half space) is piezomagnetic material $CoFe_2O_4$. Their material properties are given in tables 1 and 2 (Pan 2001). The uniform vertical surface load is $q = 1$ MPa and the radius of the loading circle is $a = 1$ m. The thickness of the first layer is $h_1 = 1$ m (unless it is redefined) and the thickness of the second layer is $h_2 \to +\infty$. Numerical results are shown in figures 2–8.

5.1. Elastic displacements and electric and magnetic potentials

Due to the axial symmetry, the displacements in any symmetric plane are the same. Their contours in the (r, z)-plane are

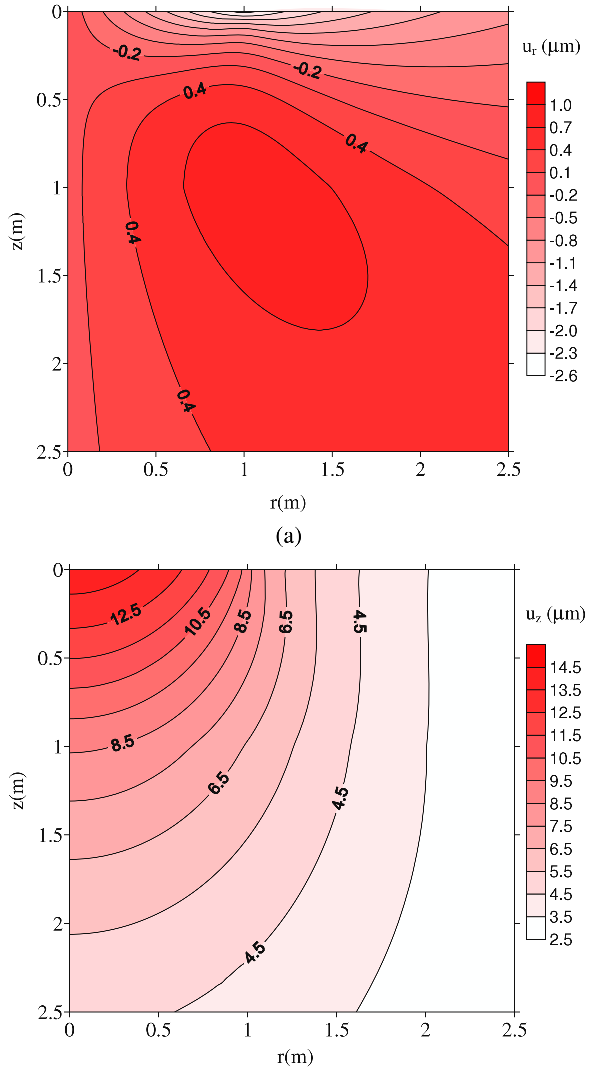

Figure 2. Contours of displacements (in μm) in the (r, z)-plane in a two-layered $BaTiO_3/CoFe_2O_4$ half space under the uniform vertical load $q = 1$ MPa over the circle of radius $a = 1$ m. The radial displacement is u_r in (a) and the vertical displacement is u_z in (b).

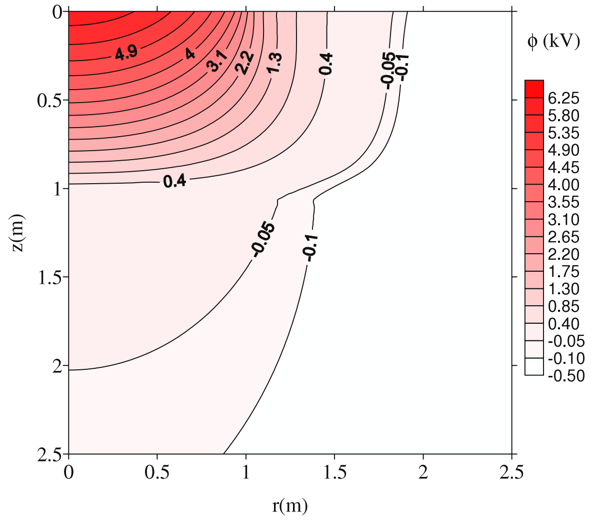

Figure 3. Contours of the electric potential ϕ (in kV) in the (r, z)-plane in a two-layered $BaTiO_3/CoFe_2O_4$ half space under the uniform vertical load $q = 1$ MPa over the circle of radius $a = 1$ m.

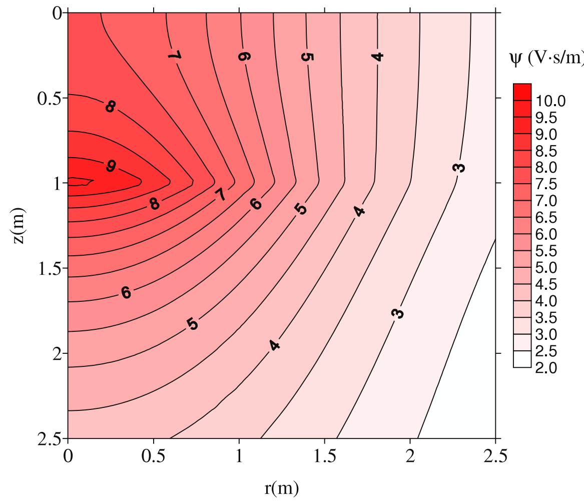

Figure 4. Contours of the magnetic potential ψ (in V s m^{-1}) in the (r, z)-plane in a two-layered $BaTiO_3/CoFe_2O_4$ half space under the uniform vertical load $q = 1$ MPa over the circle of radius $a = 1$ m.

Table 2. Nonzero material coefficients of the magnetostrictive $CoFe_2O_4$ (c_{ij} in 10^9 N m^{-2}, e_{ij} in C m^{-2}, ε_{ij} in 10^{-9} C^2 N^{-1} m^{-2}, μ_{ij} in 10^{-6} N s^2 C^{-2}).

c_{11}	c_{12}	c_{13}	c_{33}	c_{44}	μ_{11}
286	173	170.5	269.5	45.3	590
q_{31}	q_{33}	q_{15}	ε_{11}	ε_{33}	μ_{33}
580.3	699.7	550	0.08	0.093	157

shown in figure 2. The radial displacement u_r is shown in figure 2(a) and vertical displacement u_z in figure 2(b). It is interesting to note that u_z is always positive in our calculation region, and decreases with increasing distance from the loading region. Its maximum (about 14 μm) is obtained at the center of the loading circle, i.e. at point $(r, z) = (0, 0)$ (figure 2(b)). Different from the positive feature of u_z, the radial displacement u_r in figure 2(a) is negative in the region near the loading surface and positive outside. In other words, under the uniform vertical load, the structure contracts at and near the loading region, and expands outside. The minimum radial displacement is about -2.5 μm at point $(r, z) = (1$ m, $0)$, while its maximum is about 0.84 μm at point $(r, z) = (1$ m, 1 m$)$. The radial displacement u_r is zero along the z-axis in figure 2(a), which satisfies the symmetric condition of the problem. The densities of the displacement contours near the surface are larger than those far from the surface, which means that the elastic stress and strain fields in the region near the surface are larger than those in the far region.

Contours of the electric and magnetic potentials are shown, respectively, in figures 3 and 4. The electric potential decreases with increasing distance from the loading region, and its maximum is at the center of the loading circle on the surface. It is found that the density of the electric potential is quite

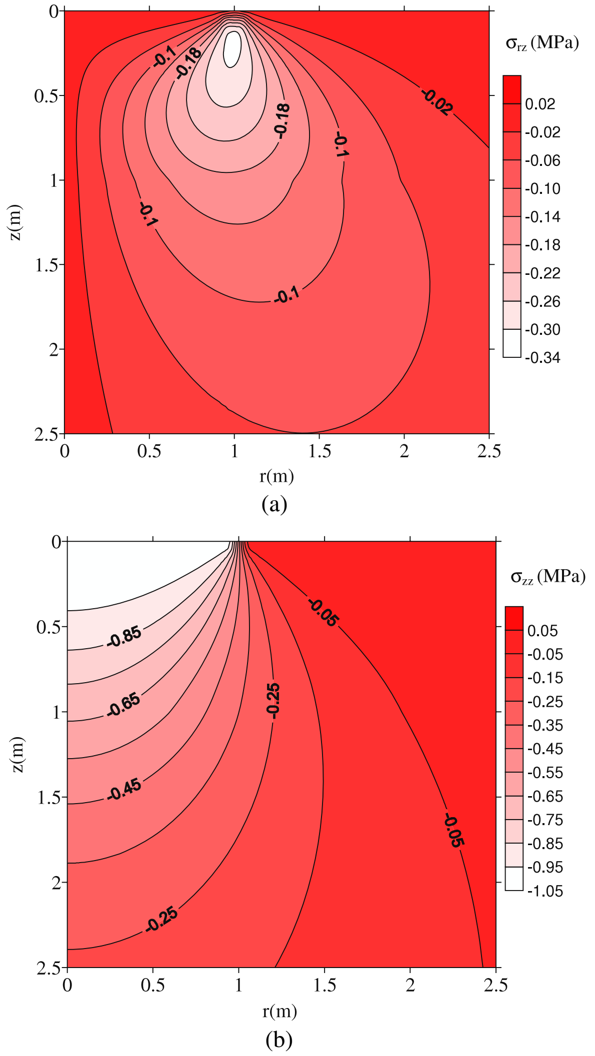

Figure 5. Contours of the stresses (in MPa) in the (r, z)-plane in a two-layered $BaTiO_3/CoFe_2O_4$ half space under the uniform vertical load $q = 1$ MPa over the circle of radius $a = 1$ m; σ_{rz} in (a) and σ_{zz} in (b).

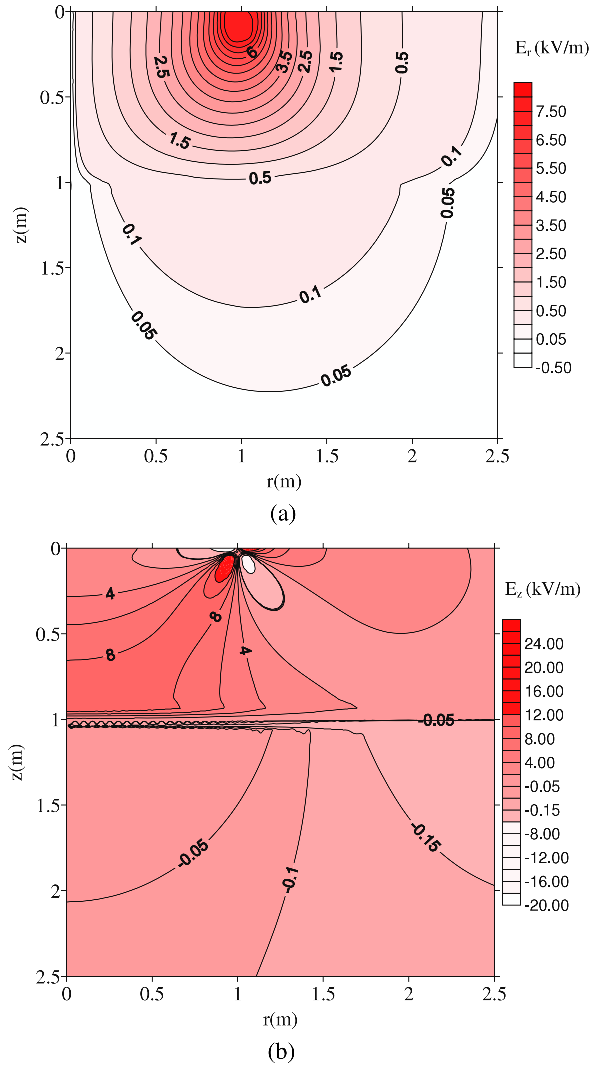

Figure 6. Contours of the electric fields (in kV m^{-1}) in the (r, z)-plane in a two-layered $BaTiO_3/CoFe_2O_4$ half space under the uniform vertical load $q = 1$ MPa over the circle of radius $a = 1$ m; E_r in (a) and E_z in (b).

low in the second (i.e. the half space) layer with very small magnitudes. This phenomenon is due to the fact that in the half space, the piezoelectric and dielectric constants are small as compared to those in the surface layer. While the electric potential reaches its maximum value on the loading surface, the magnetic potential obtains its maximum at the interface $z = 1$ m (figure 4). The maximum magnetic potential of 9.6 A is reached at point $(r, z) = (0, 1$ m$)$. The tangents of these contours are all horizontal when $r = 0$ (figures 3 and 4), consistent with the symmetry of the problem.

5.2. Stresses, electric fields, and magnetic inductions

Contours of the stresses, electric fields, and magnetic inductions in the vertical (r, z)-plane are shown in figures 5–7. According to the boundary condition on the surface, the vertical normal stress σ_{zz} on the surface should equal the applied load q inside the loading region and zero outside. The relative difference between the applied exact value and our numerical results is less than 10^{-5}, and therefore the boundary conditions are satisfied. The continuity of the traction $(\sigma_{rz}, \sigma_{zz})$ across the interface is also demonstrated in figure 5. Furthermore, the shear stress in figure 5(a) shows a concentration below the surface near the edge of the loading circle with a maximum of about 0.27 MPa. The normal stress σ_{zz} in figure 5(b) reaches its extreme magnitude of 1 MPa on the surface and gradually relaxes with increasing distance from the loading region.

The contours of the electric fields E_r and E_z are shown in figure 6. It is observed that the magnitude of the electric field in the second layer is much smaller than that in the first layer, with more than two orders of difference. This phenomenon is due to the non-piezoelectricity and low permeability of the second layer. Since $e_{ij} = 0$ and $d_{ij} = 0$ in the second layer, there will be no elastic- and magnetic-induced electric field in this layer. On the other hand, our numerical results (figure 6) show that electric field does exist in the second layer. Hence it is concluded that the electric field in the second layer is induced by the electric field in the first layer, i.e. the interplay of the

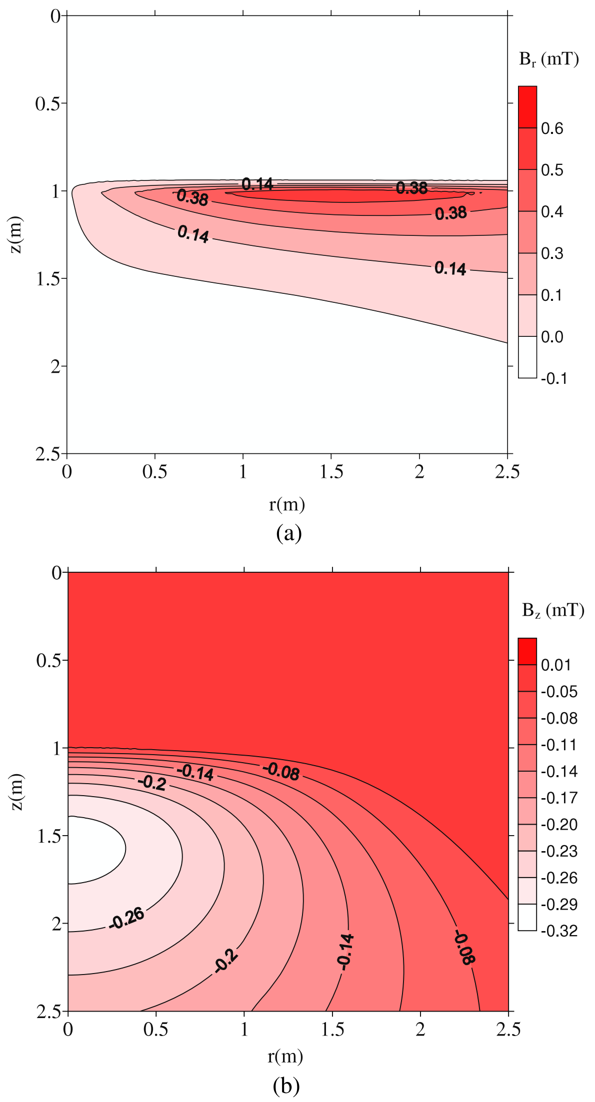

Figure 7. Contours of the magnetic inductions (in mT) in the (r, z)-plane in a two-layered $BaTiO_3/CoFe_2O_4$ half space under the uniform vertical load $q = 1$ MPa over the circle of radius $a = 1$ m; B_r in (a) and B_z in (b).

electric field between the adjacent layers is demonstrated. This is actually the product property in this novel composite where the mechanical strain serves as a bridge between the electric and magnetic fields.

Similarly, because of the non-piezomagnetic property (i.e. $q_{ij} = 0$) and non-magneto-electric coupling (i.e. $d_{ij} = 0$) in the first layer, the magnetic induction in the first layer is induced by the magnetic induction in the second layer. This indicates the interplay of the magnetic field between the two adjacent layers. As shown in figure 7, the magnetic induction in the first layer is much smaller than that in the second layer. It is interesting that while B_r decreases with increasing distance from the interface (figure 7(a)), there is a maximum magnitude of 0.30 mT in B_z at $(r, z) = (0, 1.55$ m) (figure 7(b)).

5.3. Influence of layer thickness

The influence of the thickness of the surface layer on the stress, electric field, and magnetic induction at the interface is investigated. Numerical results are shown in figure 8 for two points on the interface ($r/a = 0$ and 1).

The magnitude of the vertical normal stress σ_{zz} at the interface in general decreases with increasing thickness of the surface layer (figure 8(a)). However, when the thickness is thin enough, the stress σ_{zz} at the interface and below the loading center ($r/a = 0$) behaves abnormally. For example, it reaches its maximum magnitude 1.02 MPa when $h/a = 0.26$. Such a thickness of the surface layer may be called the critical thickness of the stress, denoted by h^{σ}_{cr}. Thus, when $0 < h < h^{\sigma}_{\mathrm{cr}}$, the magnitude of the interfacial stress below the load center increases with increasing layer thickness.

Figure 8(b) shows the variation of the interfacial electric field E_z versus the normalized thickness of the first layer h/a. Compared to the vertical normal stress σ_{zz} in figure 8(a), the distribution of E_z is much more complicated. (1) This vertical electric field is discontinuous across the interface. Its magnitude is much smaller in the surface layer (i.e. layer 1) than that in the half space (i.e. layer 2). (2) Even though the interfacial electric field is small in the surface layer, a critical thickness of the surface layer also exists. In other words, the electric field E_z will first increase its magnitude with increasing h/a. Once it reaches the maximum magnitude, it will decrease. For instance, the magnitudes for $r/a = 0$ and 1 are, respectively, $E_{z\,\max} = 1.13$ kV m^{-1} and 1.375 kV m^{-1} when $h/a = 0.055$ and 0.08. (3) The interfacial electric field E_z in the surface layer will change sign (from negative to positive) at a certain h/a ratio, and tends to zero gradually with increasing h/a. The interfacial electric field E_z is much larger in layer 2 (i.e. in the half space). It first decreases with increasing h/a. Once it reaches a minimum (at h/a very close to zero), it increases with h/a. After reaching its maximum, it then gradually decreases to zero with increasing h/a.

Variation of the interfacial magnetic induction B_z is shown in figure 8(c). The interfacial magnetic induction has the same negative sign and reaches its maximum magnitude at $h/a = 0.78$ and $h/a = 1.12$, respectively, for $r/a = 0$ and 1 (with magnitudes 4.8×10^{-5} T for $r/a = 0$ and 1.86×10^{-5} T for $r/a = 1$). After reaching its minimum, the magnetic induction will gradually decay to zero with increasing h/a.

6. Conclusions

In this paper, the magneto-electro-elastic responses of the layered multiferroic structure under uniform vertical circular load are presented. The semi-analytical solutions are obtained by means of the vector functions and the corresponding propagator matrix method. Numerical analyses for two-layered structures are carried out. The coupling effects among the elastic, electric, and magnetic fields are demonstrated. Two interesting phenomena are found in the calculated structures. One is the coupling effect between the adjacent layers, i.e. the magnetic fields (electric field) in the first layer can be induced by those in the second layer, even if the first layer has no piezomagnetic (piezoelectric) properties. The other is that an abnormal phenomenon will happen when the thickness of the surface layer is ultrathin. Since the field at the interface often plays a significant role in fracture analysis, these

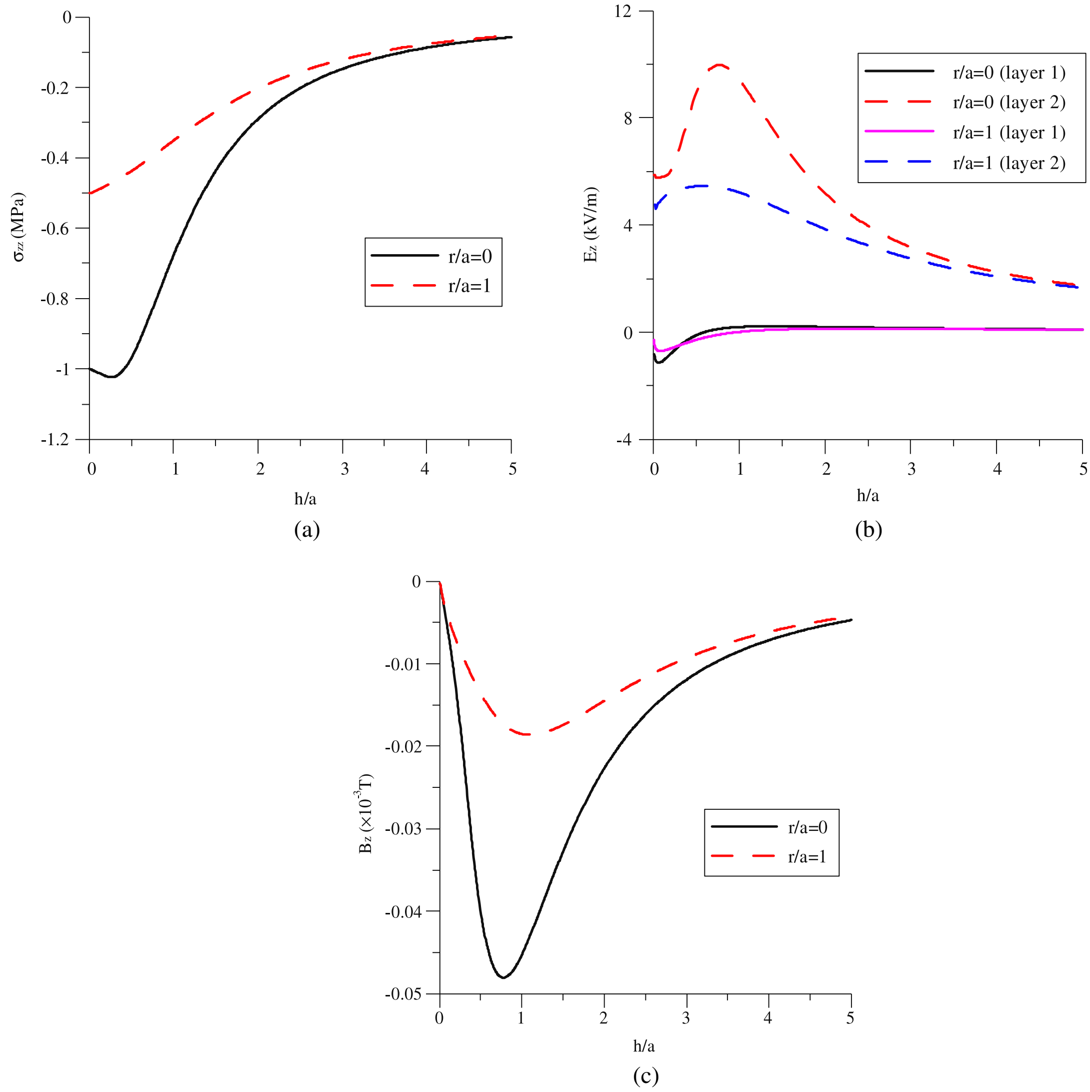

Figure 8. Field quantities at the interface ($r/a = 0$ and $r/a = 1$) versus the thickness of the surface layer h/a: σ_{zz} versus h/a in (a), E_z versus h/a in (b), and B_z versus h/a in (c).

interesting phenomena may provide future guidance for the coating design. We further point out that the proposed solution should be useful to the corresponding indentation problem and to the arbitrary surface loading case.

Acknowledgments

This work is supported by the National Natural Science Foundation (10602050) and a Jiangsu Government Scholarship for Overseas Studies.

Appendix

The nonzero components of the matrix $[\mathbf{W}_k]$ in equation (18) for the given layer k are

$$W_{12} = \frac{c_{13}d_{33}^2 + d_{33}e_{33}q_{31} + d_{33}e_{31}q_{33} - q_{31}q_{33}\varepsilon_{33} - (e_{31}e_{33} + c_{13}\varepsilon_{33})\mu_{33}}{Q}$$

$$W_{13} = \frac{d_{33}^2 - \varepsilon_{33}\mu_{33}}{Q}, \qquad W_{17} = \frac{d_{33}q_{33} - e_{33}\mu_{33}}{Q},$$

$$W_{18} = \frac{d_{33}e_{33} - q_{33}\varepsilon_{33}}{Q}, \qquad W_{21} = -1, \qquad W_{24} = \frac{1}{c_{44}},$$

$$W_{25} = -\frac{e_{15}}{c_{44}}, \qquad W_{26} = -\frac{q_{15}}{c_{44}}, \qquad W_{34} = 1$$

$$W_{52} = \frac{q_{33}(c_{13}d_{33} - e_{33}q_{31} + e_{31}q_{33}) - c_{13}e_{33}\mu_{33} + c_{33}(e_{31}\mu_{33} - d_{33}q_{31})}{Q},$$

$$W_{53} = \frac{d_{33}q_{33} - e_{33}\mu_{33}}{Q}, \qquad W_{57} = \frac{c_{33}\mu_{33} + q_{33}^2}{Q},$$

$$W_{58} = -\frac{c_{33}d_{33} + e_{33}q_{33}}{Q},$$

$$W_{62} = \frac{e_{33}(c_{13}d_{33} + e_{33}q_{31} - e_{31}q_{33}) - c_{13}q_{33}\varepsilon_{33} - c_{33}(d_{33}e_{31} - q_{31}\varepsilon_{33})}{Q},$$

$$W_{63} = \frac{e_{33}d_{33} - q_{33}\varepsilon_{33}}{Q}, \qquad W_{67} = W_{58},$$

$$W_{68} = \frac{c_{33}\varepsilon_{33} + e_{33}e_{33}}{Q}, \qquad W_{74} = \frac{e_{15}}{c_{44}},$$

$$W_{75} = -\left(\frac{e_{15}^2}{c_{44}} + \varepsilon_{11}\right), \qquad W_{76} = -\left(d_{11} + \frac{e_{15}q_{15}}{c_{44}}\right),$$

$$W_{84} = \frac{q_{15}}{c_{44}}, \qquad W_{85} = -\left(\frac{q_{15}e_{15}}{c_{44}} + d_{11}\right),$$

$$W_{86} = -\left(\frac{q_{15}^2}{c_{44}} + \mu_{11}\right),$$

$$W_{42} = c_{11} - c_{13}W_{12} - e_{31}W_{52} - q_{31}W_{62},$$

$$W_{43} = -c_{13}W_{13} - e_{31}W_{53} - q_{31}W_{63},$$

$$W_{47} = -c_{13}W_{17} - e_{31}W_{57} - q_{31}W_{67},$$

$$W_{48} = -c_{13}W_{18} - e_{31}W_{58} - q_{31}W_{68}$$

where

$$Q = c_{33}d_{33}^2 + 2d_{33}e_{33}q_{33} - q_{33}^2\varepsilon_{33} - (e_{33}^2 + c_{33}\varepsilon_{33})\mu_{33}$$

and all the material properties are those corresponding to the kth layer.

References

Balaban N Q *et al* 2001 Force and focal adhesion assembly: a close relationship studied using elastic micropatterned substrates *Nat. Cell Biol.* **3** 466–72

Becker J M and Bevis M 2004 Love's problem *Geophys. I. Int.* **156** 171–8

Benveniste Y 1995 Magnetoelectric effect in fibrous composites with piezoelectric and piezomagnetic phases *Phys. Rev.* B **51** 16424–7

Chen W Q, Lee K Y and Ding H J 2004 General solution for transversely isotropic magneto-electro-thermo-elasticity and the potential theory method *Int. J. Eng. Sci.* **42** 1361–79

Chen W Q, Pan E, Wang H M and Zhang C Z 2010 Theory of indentation on multiferroic composite materials *J. Mech. Phys. Solids* **58** 1524–51

Doherty J P and Deeks A J 2003 Elastic response of circular footings embedded in a non-homogeneous half-space *Geotechnique* **53** 703–14

Duan C G, Jaswal S S and Tsymbal E Y 2006 Predicted magnetoelectric effect in Fe/BaTiO$_3$ multilayers: ferroelectric control of magnetism *Phys. Rev. Lett.* **97** 047201

Feng W J, Pan E and Wang X 2007 Dynamic fracture analysis of a penny-shaped crack in a magnetoelectroelastic layer *Int. J. Solids Struct.* **44** 7955–74

Feng W J, Pan E, Wang X and Jin J 2009 Rayleigh waves in magneto-electro-elastic half planes *Acta Mech.* **202** 127–34

Fiebig M 2005 Revival of the magnetoelectric effect *J. Phys. D: Appl. Phys.* **38** R123–52

Giannakopoulos A E and Suresh S 1999 Theory of indentation of piezoelectric materials *Acta Mater.* **47** 2153–64

Gilbert F and Backus G 1966 Propagator matrices in elastic wave and vibration problems *Geophysics* **31** 326–32

Graig R F 1997 *Soil Mech.* (London: Taylor and Francis)

Han F, Pan E, Roy A K and Yue Z Q 2006 Responses of piezoelectric, transversely isotropic, functionally graded, and multilayered half spaces to uniform circular surface loadings *Comput. Model. Eng. Sci.* **14** 15–29

Hooper J A 1975 Elastic settlement of a circular raft in adhesive contact with a transversely isotropic medium *Geotechnigque* **25** 691–711

Hou P F, Ding H J and Chen J Y 2005 Green's functions for transversely isotropic magnetoelectroelastic media *Int. J. Eng. Sci.* **43** 826–58

Ke L L, Yang J, Kitipornchai1 S and Wang Y S 2008 Frictionless contact analysis of a functionally graded piezoelectric layered half-plane *Smart Mater. Struct.* **17** 025003

Kimura T, Goto T, Shintani H, Ishizaka K, Arima T and Tokura Y 2003 Magnetic control of ferroelectric polarization *Nature* **426** 55–8

Kohlstedt H, Pertsev N A, Contreras J R and Waser R 2005 Theoretical current–voltage characteristics of ferroelectric tunnel junctions *Phys. Rev.* B **72** 125341

Kumar P 1988 Nonhomogeneous and cross-anisotropic infinite elements *Comput. Struct.* **28** 327–33

Li J Y 2003 Uniqueness and reciprocity theorems for linear thermo-electro-magneto-elasticity *Q. J. Mech. Math.* **56** 35–43

Li J Y and Dunn M L 1998 Micromechanics of magnetoelectroelastic composite materials: average fields and effective behavior *J. Intell. Mater. Syst. Struct.* **7** 404–15

Liu G, Nan C W, Cai N and Lin Y H 2004 Calculations of giant magnetoelectric effect in multiferroic composites of rare-earth-iron alloys and PZT by finite element method *Int. J. Solids Struct.* **41** 4423–34

Liu J X, Liu X L and Zhao Y B 2001 Green functions for anisotropic magnetic-electro-elastic solids with an elliptical cavity or a crack *Int. J. Eng. Sci.* **39** 1045–418

Lottermoser T, Lonkai T, Amann U, Hohlwein D, Ihringer J and Fiebig M 2004 Magnetic phase control by an electric field *Nature* **430** 541–4

Nan C W 1994 Magnetoelectric effect in composites of piezoelectric and piezomagnetic phases *Phys. Rev.* B **50** 6082–8

Oner M 1990 Vertical and horizontal deformation of an inhomogeneous elastic half-space *Int. J. Numer. Anal. Methods Geomech.* **14** 613–29

Pan E 1989 Static response of a transversely isotropic and layered half-space to general surface loads *Phys. Earth Planet. Inter.* **54** 353–63

Pan E 2001 Exact solution for simply supported and multilayered magneto-electro-elastic plates *J. Appl. Mech.* **68** 608–18

Pan E 2002 Three-dimensional Green functions in anisotropic magneto-electro-elastic bimaterials *Z. Angew. Math. Phys.* **53** 815–38

Pan E, Bevis M, Han F, Zhou H and Zhu R 2007 Surface deformation due to loading of a layered elastic half-space: a rapid numerical kernel based on a circular loading element *Geophys. J. Int.* **88** 90–100

Pan E and Han F 2005 Green's functions for transversely isotropic piezoelectric functionally graded multilayered half spaces *Int. J. Solids Struct.* **42** 3207–33

Pang Y, Wang Y S, Liu J X and Fang D N 2010 A study of the band structures of elastic wave propagating in piezoelectric/piezomagnetic layered periodic structures *Smart Mater. Struct.* **19** 055012

Ramesh R and Spaldin N A 2007 Multiferroics: progress and prospects in thin films *Nat. Mater.* **6** 21–9

Ramirez G 2006 Frictionless contact in a layered piezoelectric medium characterized by complex eigenvalues *Smart Mater. Struct.* **15** 1287–95

Rogez G, Viart N and Drillon M 2010 Multiferroic materials: the attractive approach of metal–organic frameworks (MOFs) *Angew. Chem. Int. Edn* **49** 1921–3

Rowe R K and Booker J R 1981 The behavior of footings resting on a non-homogeneous soil mass with a crust, part II circular footings *Can. Geotech. J.* **18** 265–79

Rungamornrat J and Senjuntichai T 2009 Regularized boundary integral representations for dislocations and cracks in smart media *Smart Mater. Struct.* **18** 074010

Schwarz U S, Balaban N Q, Riveline D, Bershadsky A, Geiger B and Safran S A 2002 Calculation of forces at focal adhesions from elastic substrate data: the effect of localized force and the need for regularization *Biophys. J.* **83** 1380–94

Sih G C and Chen E P 2003 Dilatational and distortional behavior of cracks in magnetoelectroelastic materials *Theor. Appl. Fract. Mech.* **40** 1–21

Spaldin N A and Fiebig M 2005 The renaissance of magnetoelectric multiferroics *Science* **309** 391–2

Sun K H and Kim Y Y 2010 Layout design optimization for magneto-electro-elastic laminate composites for maximized energy conversion under mechanical loading *Smart Mater. Struct.* **19** 055008

Ulitko A F 1979 *Method of Special Vector Functions in Three-Dimensional Elasticity* (Kiev: Naukova Dumka) p 264 (in Russian)

Wang C D, Pan E, Tzeng C S, Han F and Liao J J 2005 Displacements and stresses due to a uniform vertical circular load in an inhomogeneous cross-anisotropic half-space *Int. J. Geomech.* **6** 1–10

Wang J H, Chen C Q and Lu T J 2008 Indentation responses of piezoelectric films *J. Mech. Phys. Solids* **56** 3331–51

Wang R, Han Q and Pan E 2010 An analytical solution for a multilayered magneto-electro-elastic circular plate under simply supported lateral boundary *Smart Mater. Struct.* **19** 065025

Wang X and Shen Y P 2002 The general solution of three-dimensional problems in magnetoelectroelastic media *Int. J. Eng. Sci.* **40** 1069–80

Wu T L and Huang J H 2000 Closed-form solutions for the magnetoelectric coupling coefficients in fibrous composites with piezoelectric and piezomagnetic phase *Int. J. Solids Struct.* **37** 2981–3009

Xu J, Zhu X and Meng Z 1999 Effect of the interdiffusion reaction on the compatibility of PZT/PNN functionally gradient piezoelectric materials *IEEE Trans. Compon. Packag. Technol.* **22** 11–6

Yu H Y 2001 A concise treatment of indentation problems in transversely isotropic half-spaces *Int. J. Solids Struct.* **38** 2213–32

Yue Z Q, Yin J H and Zhang S Y 1999 Computation of point load solutions for geo-materials exhibiting elastic non-homogeneity with depth *Comput. Geotech.* **25** 75–105

Zhong X C 2009 Analysis of a dielectric crack in a magnetoelectroelastic layer *Int. J. Solids Struct.* **46** 4221–30

Zhong X C, Liu F and Li X F 2009 Transient response of a magnetoelectroelastic solid with two collinear dielectric cracks under impacts *Int. J. Solids Struct.* **46** 2950–8

Zhong X L, Liao M, Wang J B, Xie S H and Zhou Y C 2008 Structural, ferroelectric, ferromagnetic, and magnetoelectric properties of the lead-free $Bi_{3.15}Nd_{0.85}Ti_3O_{12}/CoFe_2O_4$ double-layered thin film *J. Cryst. Growth* **310** 2995–8

Zhuravlev M Y, Sabirianov R F, Jaswal S S and Tsymbal E Y 2005 Giant electroresistance in ferroelectric tunnel junctions *Appl. Phys. Lett.* **94** 246802